Int. J. Solids Structures Vol. 26, No. 3, pp. 313–330, 1990
Printed in Great Britain.

0020–7683/90 $3.00 + .00

DELAMINATION FAILURE OF LAYERED COMPOSITE PLATES LOADED IN COMPRESSION

D. BRUNO
Dipartimento di Strutture, Università della Calabria, Italy

and

A. GRIMALDI
Facoltà di Ingegneria Civile Edile, II Università di Roma, Via Orazio Raimondo, 00173 Rome, Italy

(*Received* 18 *November* 1987; *in revised form* 2 *February* 1989)

Abstract—In this paper, we analyze the delamination of two-layer plates loaded in compression. An initial defect of adhesion between the layers is assumed, and the propagation of the delamination produced by the buckling of the debonded area is studied. The brittle fracture mechanics approach is used to model the debonding phenomenon and the analytical solution is derived from it. The results are then compared with those obtained by means of a finite element approach, in which the layers' adhesion is modeled with unilateral springs.

1. INTRODUCTION

Plates laminated in orthotropic layers are increasingly used in aerospace, civil and mechanical engineering structures. If the edges of laminates are not secured properly, delamination can occur. It can either be due to the presence of normal tensile stresses or to the imperfect bonding between layers. In the latter case, delamination can propagate especially if loads transverse to the laminate, or normal compression are applied. Delamination induced by buckling of layers can greatly influence the failure characteristic of compressively-loaded laminated plates as shown by various authors (Early, 1981; Sterness and Williams, 1983; Chai *et al.*, 1981; Evans and Hutchinson, 1984). In this paper a unilateral contact approach, developed in previous studies by Grimaldi and Reddy (1982) and Ascione and Bruno (1983), is used to model the propagation of delamination of two-layer plates under uniform axial compression.

The adhesion strength between layers is modeled by springs with finite tensile strength. The plate is modeled according to the Von Karman plate theory.

A finite element model is developed and applied to investigate some examples of buckling delamination of two-layer plates with specified initial bonding defect.

For the case of one-dimensional delamination the present approach is validated by comparing finite element results with analytical solutions. The relationship between the brittle fracture mechanics approach and the present approach is also discussed.

2. BUCKLING INDUCED DELAMINATION

In this section we present two example problems of delamination of two-layer plates. The first one corresponds to a narrow two-layer plate of length L and width b ($L/b \gg 1$), with a symmetrical initial bonding defect of length l_0, and subjected to axial compression (Fig. 1a,b). The second example problem refers to a two-layer symmetrically laminated circular plate of radius R with a concentric penny-shaped bonding defect of radius R_0, and subjected to a uniform compressive stress at the edge (Fig. 1c,d).

As the compressive load N increases several instability phenomena can occur related to the plate geometry (layer-thickness ratio, initial defect size and plate size). With small initial defects an overall instability phenomenon of the plate can be found which is scarcely affected by the delamination defect.

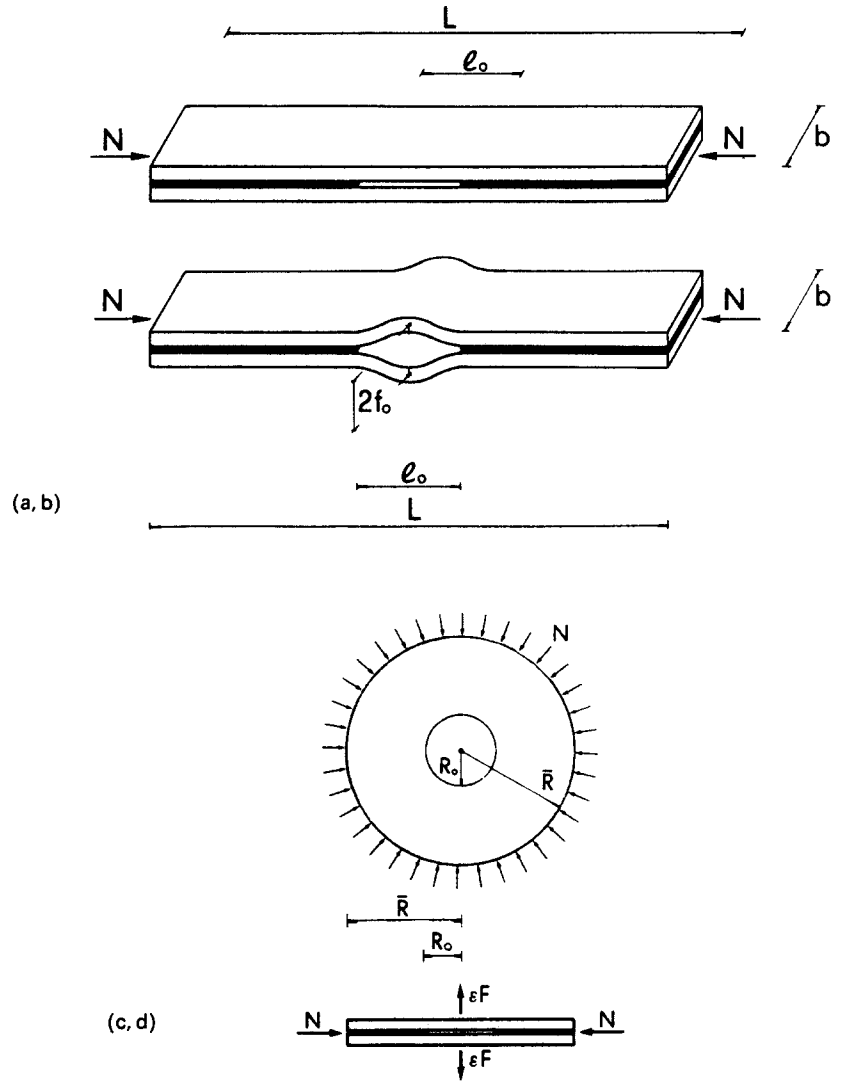

Fig. 1. Narrow plate example (a, b). Circular plate example (c, d).

On the contrary, when considerable initial defect size occurs, the layers buckle in the initial delaminated area (which may subsequently spread). This phenomenon becomes particularly interesting when a geometric or load imperfection is also present in the delaminated region (Fig. 1b,d). Finally, when different thicknesses of layers are given, a global instability of the whole plate can occur together with a local instability of the layers. For the narrow-plate model some detailed results were obtained by Yin *et al.* (1986), where an analytical model was used to study the critical and postcritical behaviour of a two-layer plate with different layer thicknesses and an arbitrary size of initial defect.

The circular-plate model was studied by Bottega and Maewal (1983) by using an analytical model.

In this paper the analysis is restricted to the case of symmetric two-layer plates under the assumption that the ratio of plate size to defect is such that a local instability phenomenon occurs.

In particular, for our example problems (Fig. 1), we observe that, by increasing N, the transverse displacements of the initial delaminated region increase until a characteristic value N_{lim} of the load is reached, a value which defines the starting point of the layers' delamination. After reaching this limit point the spreading of the delaminated area is unstable, that is, the equilibrium configurations for $l > l_0$ ($R > R_0$) correspond to decreasing values of the load N (Fig. 2a,b).

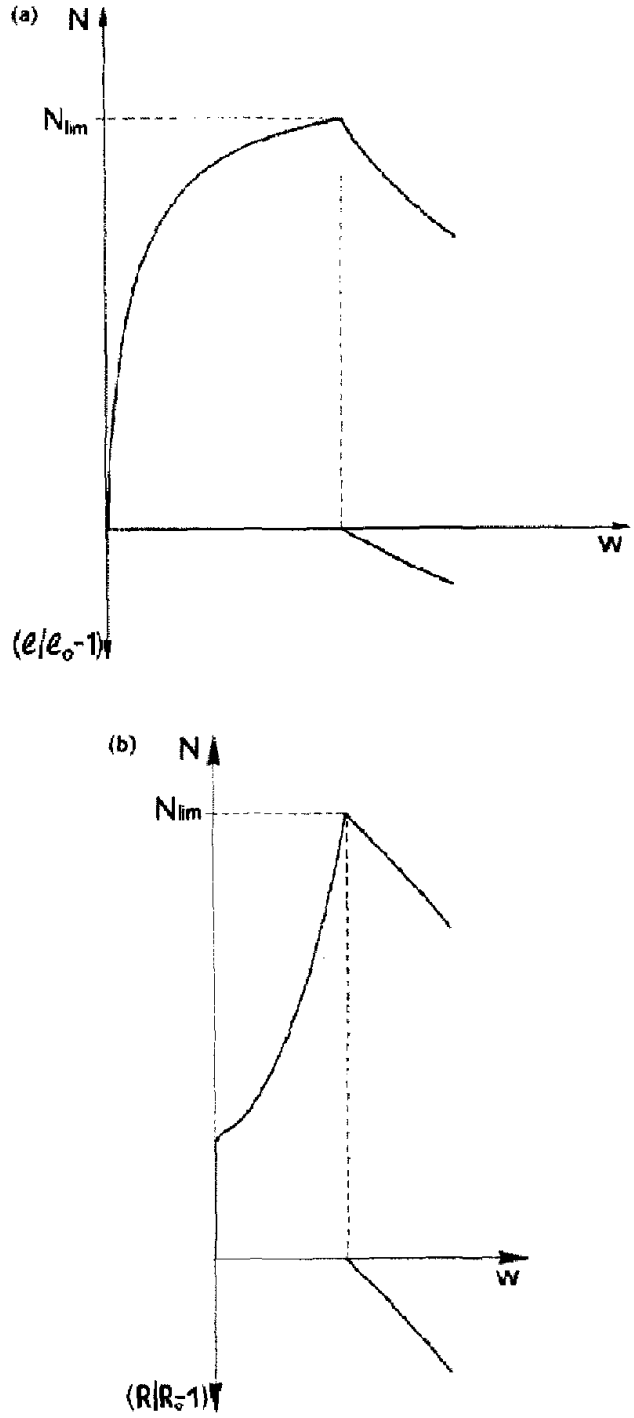

Fig. 2. Narrow plate (a), circular plate (b). Axial force versus transverse deflection before and after delamination propagation.

The present paper aims at demonstrating the possibility of using two different approaches in the analysis of the delamination problem.

In the first approach the delamination is studied by utilizing the results of fracture mechanics; in the second, the adhesion between the layers is simulated by an elastic foundation with finite bonding strength.

In the second approach a numerical analysis is developed by using a finite element technique. The comparison between analytical and numerical results shows the effectiveness of the numerical approach which can also be applied to more complicated two-dimensional problems.

3. FRACTURE MECHANICS APPROACH

In the fracture mechanics approach the adhesion between the layers is characterized by the surface energy density Γ. Moreover, the delamination is assumed to occur when the energy release equals the adhesion surface energy, that is:

$$G = \gamma. \tag{1}$$

Here G and γ denote the potential energy release and the surface adhesion energy per unit length of the advancing opening, respectively.

3.1. *First example problem: narrow plate*

In this case relation (1) becomes:

$$-\frac{\partial}{\partial l}\Delta\Phi = \Gamma b \tag{2}$$

where $\Delta\Phi$ is the increment of the total potential energy from the fundamental equilibrium path, and l is the length of the debonded area. In order to give an expression for $\Delta\Phi$, we now observe that our problem is geometrically nonlinear owing to the destabilizing effect of the axial load.

Hence, in the present case (one-dimensional example), if we assume that the narrow plate is axially inextensible, the increment of the total potential energy $\Delta\Phi^*$ of the perfect structure (Fig. 1a) is given by:

$$\Delta\Phi^*(\theta, \lambda) = \tfrac{1}{2}EI\int_0^l \left(\frac{\mathrm{d}\theta}{\mathrm{d}s}\right)^2 \mathrm{d}s - \lambda\int_0^l (1-\cos\theta)\,\mathrm{d}s \tag{3}$$

where θ is the bending slope, s is the arc length along the plate axis, EI is the flexural rigidity of the plate, λ is the load parameters and l is the actual opening length.

If an initial small imperfection is also present (Fig. 1b), the increment of the total potential energy $\Delta\Phi$ of the imperfect structure can be expressed as:

$$\Delta\Phi(\theta, \lambda) = \Delta\Phi^*(\theta, \lambda) + \lambda\varepsilon I(\theta) \tag{4}$$

where the parameter ε characterizes the value of the imperfection and $I(\theta)$ is a functional related to the geometrical imperfection.

The functional $I(\theta)$, for small initial imperfections is expressed by:

$$I(\theta) = \int_0^l \theta_0 \sin\theta\,\mathrm{d}s \tag{5}$$

where $\theta_0(s)$ is the function which defines the geometric imperfection.

We point out that the functionals (3) and (4) refer to the upper layer only, since we can restrict our attention to it because of symmetry.

The equilibrium configurations of the imperfect structure, defined by eqn (4), can be studied by utilizing a perturbative approach in the form presented by Budiansky (1974).

Let us denote by λ_c the critical value of the applied loads, with $\theta_c(s)$ the buckling mode [corresponding to the transverse displacements $w_c(s)$] and with ξ the dimensionless displacement parameter:

$$\xi = \frac{w(l/2)}{l}. \tag{6}$$

Then, the equilibrium configurations of the structure are defined by means of the equation:

$$\left(\frac{\lambda}{\lambda_c}-1\right)\varepsilon-\tfrac{1}{8}\xi^3+\frac{\lambda}{\lambda_c}\varepsilon\mu=0 \tag{7}$$

where:

$$\mu=\frac{1}{2}\frac{I'\theta_c}{\Phi_c''\theta_c^2}=\frac{1}{2}\frac{\int_0^l\theta_c\theta_0\,ds}{\int_0^l\theta_c^2\,ds}. \tag{8}$$

In the previous equation the term $I'\theta_c$ denotes the differential of the functional $I(\theta)$, evaluated in the critical direction θ_c and $\Phi_c''\theta_c^2$ denotes the derivative, with respect to the load parameter λ, of the second differential $\Phi_c''\theta_c^2$ of the total potential energy, evaluated at the bifurcation point. If we assume an initial geometrical imperfection, as the one depicted in Fig. 3, and assume as imperfection parameter:

$$\varepsilon=f_0/l_0 \tag{9}$$

we have:

$$I'\theta_c=-2l\left[1+\cos\pi\left(1-\frac{l_0}{l}\right)\right]. \tag{10}$$

It can be observed that the effects of the geometric imperfection are revealed through the quantity $I'\theta_c$. Therefore, the shape of the geometric imperfection $\theta_0(s)$ is not particularly important to subsequent developments because the relative effects can be easily evaluated by the integral (5).

The energy increment $\Delta\Phi$ can be expressed in the form:

$$\Delta\Phi(\theta,\lambda)=-\frac{l^3}{4EI}(\lambda-\lambda_c)^2+\lambda\varepsilon\xi I'\theta_c. \tag{11}$$

Then, by using eqns (2), (7) and (11), we give the following expression for the delamination condition:

$$\tfrac{3}{16}\xi^4+2\xi^2+\varepsilon B(\xi)=\alpha \tag{12}$$

where:

$$\alpha=4\Gamma b/\pi^2\lambda_c \tag{13}$$

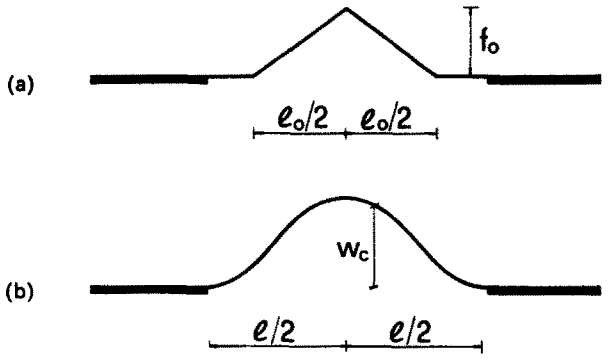

Fig. 3. (a) Initial imperfection. (b) Buckling mode.

$$B(\xi) = -\left(\frac{A(l)}{\pi^2} - \tfrac{1}{16}\mu\right)\xi^3 - \left(\frac{8A(l)}{\pi^2} - \mu\right)\xi - \frac{\alpha\mu}{\xi} \tag{14}$$

and

$$A(l) = \frac{\pi l_0}{l}\sin\pi\left(1 - \frac{l_0}{l}\right) - \cos\pi\left(1 - \frac{l_0}{l}\right) - 1. \tag{15}$$

The set of eqns (7) and (12) defines the equilibrium curve λ–ξ and the relation ζ–ξ, ζ being a dimensionless parameter related to the actual opening length: $\zeta = l/l_0 - 1$.

3.2. *Second example problem: circular plate*

For the second example problem we refer to the one-dimensional scheme given in Fig. 4, where the radius R is relative to the actual debonded area. Owing to symmetry, we consider the upper layer only (Fig. 4d) also in this case.

In this case the analysis of the delamination process is developed in two steps. In the first step we determine the relation between the axial stress σ_R at the boundary of the actual debonded area (radius R), and the displacements $u(r)$, $w(r)$ $(0 \leqslant r \leqslant R)$.

In the second step we analyze the annular region $R \leqslant r \leqslant \bar{R}$, and express the external uniform pressure σ and the boundary displacements $u_{\bar{R}} = u(\bar{R})$ as functions of the stress σ_R and the displacements of the circular debonded region. Hence, by using eqn (1), we obtain an equation analogous to (12), expressing the delamination condition.

The first step can be developed by assuming that the main aspects of the delamination process can be adequately modeled by the classical Von Karman's geometrically nonlinear plate theory.

Consequently, the total potential energy of the actual debonded layer can be expressed by:

$$\Phi^*(u, w, \sigma_R) = \pi D\int_0^R \left[w''^2 + 2\nu w''\frac{w'}{r} + \left(\frac{w'}{r}\right)^2\right] r\,dr$$

$$+\pi C\int_0^R \left[(u' + \tfrac{1}{2}w'^2)^2 + 2\nu(u' + \tfrac{1}{2}w'^2)\frac{u}{r} + \left(\frac{u}{r}\right)^2\right] r\,dr + 2\pi R l\sigma_R u_R \tag{16}$$

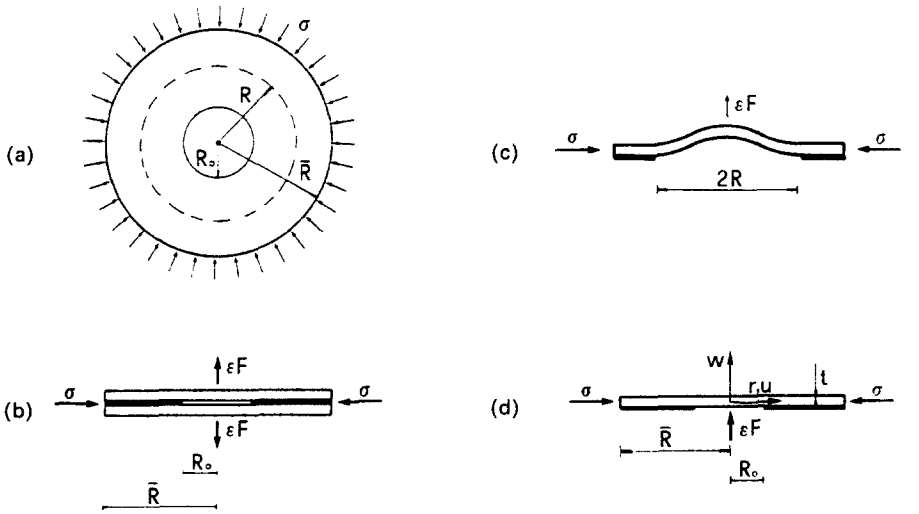

Fig. 4. Circular plate delamination problem. R_0: initial debonding radius. R: actual delamination radius.

where $D = Et^3/12(1-\nu^2)$ and $C = Et/(1-\nu^2)$ are the flexural and axial stiffnesses of the layer and ν is Poisson's ratio.

For a given value of the load, the total potential energy in an unbuckled equilibrium configuration is expressed by:

$$\Phi^0(u_0, 0, \sigma_R) = \pi C \int_0^R \left[u_0'^2 + \frac{2\nu}{r} u_0' u_0 + \left(\frac{u_0}{r}\right)^2 \right] r \, dr + 2\pi R t \sigma_R u_0(R) \tag{17}$$

where:

$$u_0(r) = -\frac{\sigma_R(1-\nu)}{E} r, \quad 0 \leqslant r \leqslant R. \tag{18}$$

Hence, the increment of the total potential energy $\Delta\Phi^*$ from the fundamental path is given by:

$$\Delta\Phi^* = \Phi^* - \Phi^0. \tag{19}$$

If a small initial imperfection is also present the increment of the total potential energy $\Delta\Phi$ of the imperfect structure can be expressed by a relation analogous to (4).

Also in this case the analysis is carried out by using a perturbative approach.

The equilibrium configurations of the actual debonded layer are characterized by the equation:

$$\left(\frac{\sigma_R}{\sigma_c} - 1\right)\xi - \frac{\sigma_2}{\sigma_c}\xi^3 + \frac{\varepsilon F}{\sigma_c}\mu = 0 \tag{20}$$

where σ_c is the critical value of the stress σ_R at the boundary of the debonded layer, σ_2 is the second-order term in the asymptotic expansion of σ_R, ξ the dimensionless displacement parameter:

$$\xi = w(0)/t; \tag{21}$$

F is the load imperfection parameter that, in the present case, we assume to be such that the corresponding central deflection of the plate is equal to t:

$$F = 16\pi D t/\bar{R}^2, \tag{22}$$

and μ is given by an equation analogous to (8) in which θ_c is replaced by the out-plane buckling mode w_c of the layer and $I'\theta_c$ by the work of the load imperfection εF on the buckling mode w_c.

To get the quantities involved in eqn (20) we utilize the results of the buckling and postbuckling analysis of the circular plate, given by Thompson and Hunt (1973, Chapter 7, pp. 168–170). For the load terms σ_c and σ_2 we have:

$$\sigma_c = 14.68\frac{D}{R^2 t}, \quad \sigma_2 = 0.2049\sigma_c; \tag{23}$$

while for the out-plane buckling mode $w_c(r)$ we have:

$$w_c(r) = \frac{J_0(\gamma R) - J_0(\gamma r)}{J_0(\gamma R) - 1}, \quad \gamma = \sqrt{\frac{\sigma_c t}{D}} = 3.832/R. \tag{24}$$

Hence, the parameter μ involved in eqn (20), is given by:

$$\mu = \frac{1}{\pi t^2} \frac{[J_0(\gamma R) - 1]^2}{(\gamma R)^2 J_0^2(\gamma R)}. \tag{25}$$

In previous equations, J_0 represents the first kind Bessel function of order zero.

The axial displacement $u_R = u(R)$, at the boundary of the delaminated area, is expressed by:

$$u(R) = u_F(R) + \xi^2 t^2 u_2(R) \tag{26}$$

where:

$$u_F(R) = -\frac{\sigma_R}{E}(1-\nu)R, \quad u_2(R) = -\frac{\gamma^2 R J_0^2(\gamma R)}{4[J_0(\gamma R) - 1]^2}, \tag{27}$$

u_F and u_2 being the prebuckling fundamental solution and the in-plane second-order displacements of the buckled configuration. Hence, we give the final expression of u_R:

$$u_R = -\frac{t^2}{R}\left[\frac{1.223}{(1+\nu)}\frac{\sigma_R}{\sigma_c} + \xi^2(\gamma R)^2 \frac{J_0^2(\gamma R)}{4[J_0(\gamma R) - 1]^2}\right]. \tag{28}$$

At this point we analyze the annular region represented in Fig. 5.

The axial displacements u of this region are expressed by:

$$u(r) = \frac{1}{E}\left[-\frac{(1+\nu)}{r}\frac{R^2(\sigma - \sigma_R)}{1-(R^2/\bar{R}^2)} + \frac{\sigma_R(R^2 - \bar{R}^2) - \sigma}{1-(R^2/\bar{R}^2)}(1-\nu)r\right], \quad R \leqslant r \leqslant \bar{R}. \tag{29}$$

Imposing that $u(R) = u_R$ and taking into account eqn (28), we give the expressions for the external pressure σ and the axial displacement $u_{\bar{R}} = u(\bar{R})$:

$$\frac{\sigma}{\sigma_c} = 1 + \frac{\bar{\sigma}_2}{\sigma_c}\xi^2 - \frac{\varepsilon F \mu}{\sigma_c \xi}. \tag{30}$$

$$u_{\bar{R}} = -\frac{\sigma(1-\nu)}{E}\bar{R} - \frac{t^2}{\bar{R}}\frac{J_0^2(\gamma R)}{4[J_0(\gamma R) - 1]^2}(\gamma R)^2 \xi^2 \tag{31}$$

where:

$$\frac{\bar{\sigma}_2}{\sigma_c} = \frac{\sigma_2}{\sigma_c} + 0.4087(1-\nu^2)\left(1 - \frac{R^2}{\bar{R}^2}\right)\frac{J_0^2(\gamma R)}{4[J_0(\gamma R) - 1]^2}(\gamma R)^2. \tag{32}$$

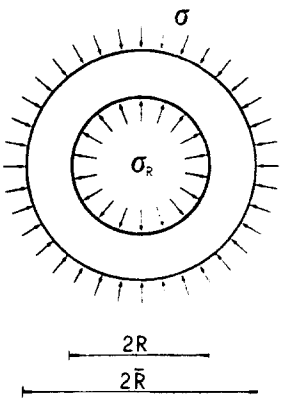

Fig. 5. σ = pressure at the plate edge of radius $\bar{R}$. σ_R = pressure at the delamination front of radius R.

The increment of the total potential energy of the whole plate is given by:

$$\Delta\Phi = -\frac{3\pi R^2 t}{E}(1-\nu^2)\frac{\sigma_c}{\bar{\sigma}_2}\frac{J_0^2(\gamma R)}{[J_0(\gamma R)-1]^2}(\sigma-\sigma_c)^2 - \varepsilon F\xi t. \tag{33}$$

In the present case the delamination condition (1) becomes:

$$-\frac{\partial}{\partial R}\Delta\Phi = 2\pi R\Gamma. \tag{34}$$

Hence, from eqns (33), (34) and (30), by using the numerical value of the Bessel function $J_0(\gamma R)$ for γR given by eqn (23), we have:

$$0.605[0.2049+0.1236(1-\nu^2)]\xi^4 + 1.21\xi^2 + O(\varepsilon^2) = 2\beta_0\left(\frac{R}{\bar{R}}\right)^4 \tag{35}$$

where:

$$\beta_0 = \frac{\Gamma\bar{R}^2}{\bar{\sigma}_c t^3}, \quad \bar{\sigma}_c = \frac{14.68D}{\bar{R}^2 t}. \tag{36}$$

The first nonzero load imperfection term in eqn (35) is of order ε^2, while in the case of the narrow-plate example, the contribution of the geometric imperfection is represented by a linear term in ε. Therefore, in the case of the circular-plate example, the influence of the considered initial load imperfection on the delamination condition becomes less important than in the case of the narrow-plate example. Moreover, previous numerical experiments showed that this term $[O(\varepsilon^2)]$ can be neglected for the evaluation of the ζ parameter.

From eqns (20), (30) and (35) we obtain the equilibrium curves σ–ξ and σ_R–ξ and the relation ζ–ξ, ζ being a dimensionless parameter related to the actual opening radius: $\zeta = R/R_0 - 1$. Moreover, through eqns (28) and (31) we obtain the force–displacements relations $\sigma_R - u_R$, $\sigma - u_R$.

4. UNILATERAL CONTACT APPROACH

In the unilateral contact approach, the adhesion between the two layers is modeled by an elastic foundation with finite tensile strength. The spring reaction r is a function of the transverse displacements w (Fig. 6):

$$r(w) = \begin{cases} kw & \text{if } w \leqslant w_0 \\ 0 & \text{if } w > w_0 \end{cases} \tag{37}$$

where k is a positive constant.

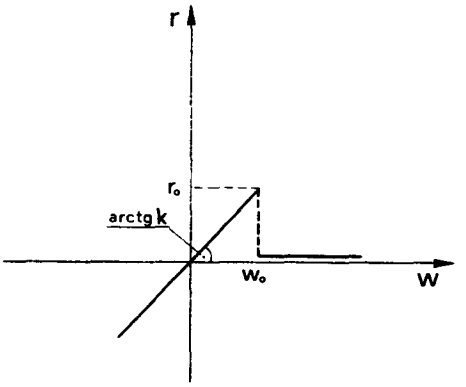

Fig. 6. Unilateral springs response: reaction versus deflection.

Therefore, the strain energy cannot exceed $U_0 = 1/2kw_0^2$ in tension. When the strain energy of the foundation equals U_0, delamination of the layers occurs. The relation between U_0 in the present approach and Γ in the fracture mechanics approach is given by $U_0 = \Gamma$. Hence, the limit elongation w_0 of the springs is given by:

$$w_0 = \sqrt{\frac{2U_0}{k}} = \sqrt{\frac{2\Gamma}{k}}. \tag{38}$$

For a given material, characterized by the limit strain energy U_0, if $k \to \infty$ the unilateral solution converges to the fracture mechanics solution.

5. NUMERICAL RESULTS

In this section we give some numerical applications relative to the two example problems examined in Section 3. In particular, some comparisons between the analytical solutions, obtained via fracture mechanics, and the numerical ones, obtained by the unilateral contact approach, are given.

5.1. *First example problem*

We refer to the scheme represented in Fig. 1b with the initial geometric imperfection shown in Fig. 3. First we give some results obtained analytically via fracture mechanics.

These results are shown in Fig. 7 and correspond to some values of the adhesion energy dimensionless parameter α_0:

$$\alpha_0 = 4\Gamma b/\pi^2 \lambda_{co}, \tag{39}$$

where:

$$\lambda_{co} = 4\pi^2 EI/l_0^2. \tag{40}$$

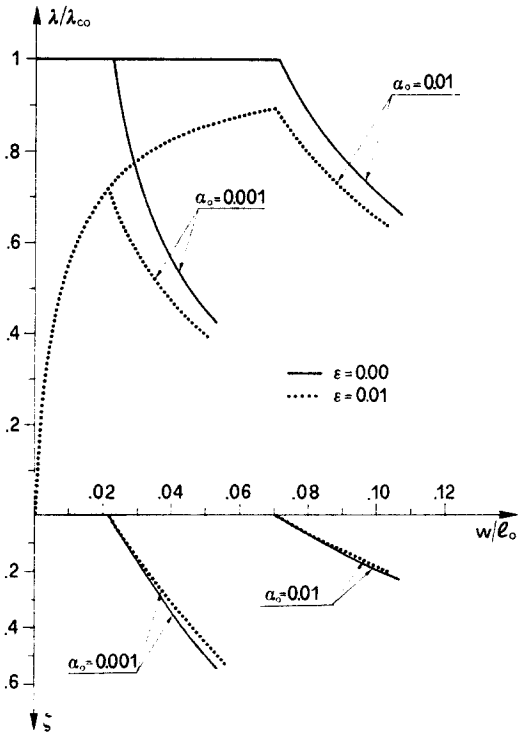

Fig. 7. Narrow plate: analytical solution. Load λ and opening delamination parameter ζ versus transverse deflection w.

In Fig. 7 the relation between the axial load λ and the central transverse deflection of the buckled region of the plate is shown. The continuous curves correspond to the case of a plate without geometric imperfection. In this case the delamination starts for a value of the axial load almost equal to the buckling load of the initial debonded region. This value defines the maximum load capacity of the plate, because the propagation of the delamination is unstable, i.e. occurs under decreasing load as shown in Fig. 7. The effect of an initial geometric imperfection, parameter ε, is also shown in Fig. 7. We observe the strong influence of initial imperfections on the maximum load capacity of the plate. Obviously, this limit value is an increasing function of the adhesion energy parameter α_0.

As far as the numerical applications corresponding to the unilateral contact approach are concerned, we developed a finite element model based on the following assumptions:

(i) axial extensibility of the narrow plate,
(ii) piece-wise linear approximation of the axial displacements u,
(iii) piece-wise cubic approximation of the transverse displacements w.

Due to symmetry, only the upper layer needs to be discretized by finite elements.

By using the results of the Von Karman thin plate theory the total potential energy of the one-dimensional narrow plate can be expressed by:

$$\Phi = \sum_{N_e} \left\{ \tfrac{1}{2}EA \int_{L_e} (u' + \tfrac{1}{2}w''^2)^2 \, dx + \tfrac{1}{2}EI \int_{L_e} w''^2 \, dx + \tfrac{1}{2}b \int_{L_e} k(w) w^2 \, dx - \int_{L_e} q_u u \, dx - \int_{L_e} q_w w \, dx \right\} \quad (41)$$

where N_e is the number of elements, EA is the axial stiffness of the layer, q_u and q_w are the axial and transverse loads and x is an abscissa along the plate axis.

The stationary condition of the functional (41) leads to the equilibrium equations in discrete form:

$$\mathscr{R} - \mathscr{Q} = \mathbf{0} \quad (42)$$

where $\mathscr{R}$ and $\mathscr{Q}$ are the vectors of the resultant internal and external nodal forces, respectively. The elemental contributions $\mathscr{R}^{(e)}$ and $\mathscr{Q}^{(e)}$ of the plate element are given by:

$$\mathscr{R}_e = \begin{Bmatrix} EAL_e \varepsilon^{(e)} \mathbf{f}'_u \\ [K_1^{(e)} + EA\varepsilon^{(e)} K_2^{(e)} + K_k^{(e)}] \mathbf{w}^{(e)} \end{Bmatrix}, \quad \mathscr{Q}^{(e)} = \begin{Bmatrix} \int_{L_e} q_u \mathbf{f}_u \, dx \\ \int_{L_e} q_w \mathbf{f}_w \, dx \end{Bmatrix} \quad (43)$$

where $\mathbf{w}^{(e)}$ is the element nodal transverse displacement vector, $\varepsilon^{(e)}$ is the mean stretching and L_e is the length of the element.

$$\varepsilon^{(e)} = \frac{1}{L_e} \int_{L_e} (u' + \tfrac{1}{2}w'^2) \, dx.$$

$\mathbf{f}_u$ and $\mathbf{f}_w$ are the interpolating function vectors and the element matrices $\mathbf{K}_1^{(e)}$, $\mathbf{K}_2^{(e)}$ and $\mathbf{K}_k^{(e)}$ are expressed by:

$$\mathbf{K}_1^{(e)} = EI \int_{L_e} \mathbf{f}''_w \mathbf{f}''^{\mathrm{T}}_w \, dx, \quad \mathbf{K}_2^{(e)} = \int_{L_e} \mathbf{f}'_w \mathbf{f}'^{\mathrm{T}}_w \, dx \quad (44)$$

$$\mathbf{K}_k^{(e)} = \sum_{N_G} k P_G \mathbf{f}_w(x_e) \mathbf{f}_w^{\mathrm{T}}(x_e) \quad (45)$$

where N_G is the number of Gauss points of the eth element and the coefficients P_G are defined as:

$$P_G = \begin{cases} W_G \text{ (Gaussian weight at point } x_e) & \text{if } w(x_e) = \mathbf{f}_w^T \mathbf{w}^{(e)} < w_0 \\ 0 & \text{if } w(x_e) = \mathbf{f}_w^T \mathbf{w}^{(e)} \geq w_0. \end{cases} \tag{46}$$

The solution of the unilateral contact problem is obtained by solving a sequence of bilateral problems in which the matrix $\mathbf{K}_k^{(e)}(w)$ at the ith step sequence is evaluated from the displacement solution w_{i-1} of the previous bilateral problem.

The numerical results obtained are shown in Figs 8 and 9. The dimensionless parameter:

$$\tau = kl_0^4 b/EI \tag{47}$$

defines the relative stiffness between plate and elastic foundation.

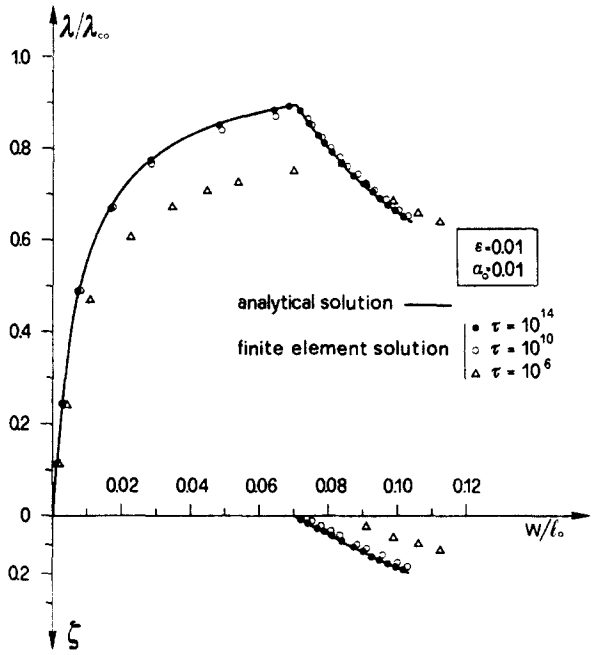

Fig. 8. Narrow plate: influence of the parameter τ on the numerical solution.

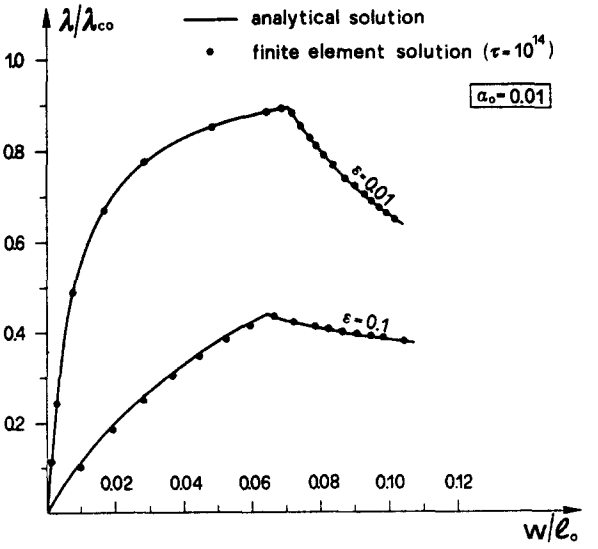

Fig. 9. Narrow plate: comparison between analytical and numerical results.

The strong influence of this parameter on the unilateral solution is shown in Fig. 8 where it is possible to observe that as $\tau \to \infty$, the unilateral solution converges to that obtained via fracture mechanics.

In Fig. 9 the influence of the imperfection parameter ε on the delamination phenomenon is shown, and a comparison between analytical and numerical results is given.

5.2. *Second example problem*

For this example problem numerical results are obtained for $\nu = 0.3$ and $t/2\bar{R} = 0.01$. Also in this case we firstly present the results obtained via fracture mechanics.

In Fig. 10 the relation between the load σ at the plate edge and the central transverse deflection w of the plate is shown. Figure 11 shows the relation between σ and the axial displacement $u_{\bar{R}}$. In this example the ratio $R_0/\bar{R}$ is assumed as $R_0/\bar{R} = 0.4$, and two different values of the adhesion energy parameter β_0 are considered.

These figures show that, by increasing the load, the delamination process starts from a buckled equilibrium configuration of the initial debonded area, corresponding to a value of the load which can be much greater than the buckling load. This behaviour is due to high stiffness of the circular plate in the postbuckling equilibrium configurations. We point out the different behaviour of this example with respect to the narrow plate.

After starting, the delamination grows with decreasing load with a very unstable behaviour.

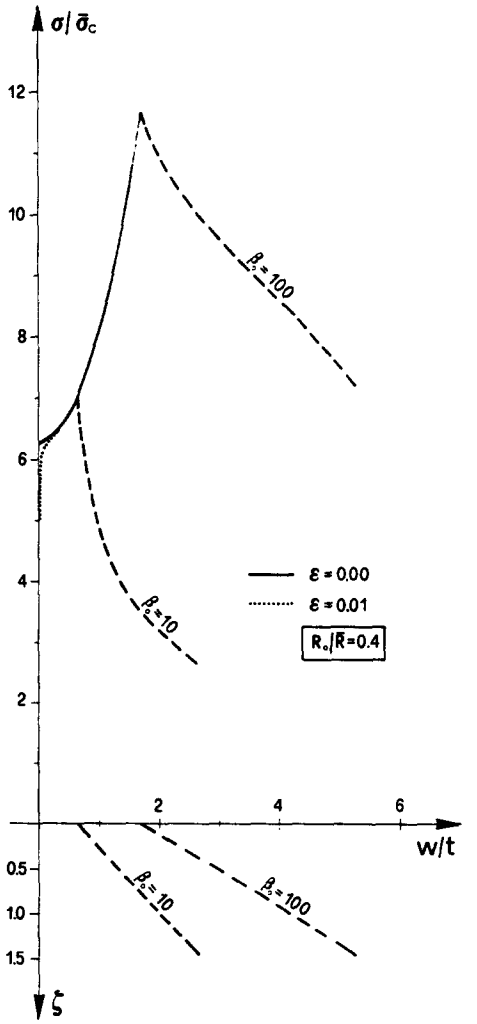

Fig. 10. Circular plate: analytical solution. External pressure edge σ versus central transverse deflection w.

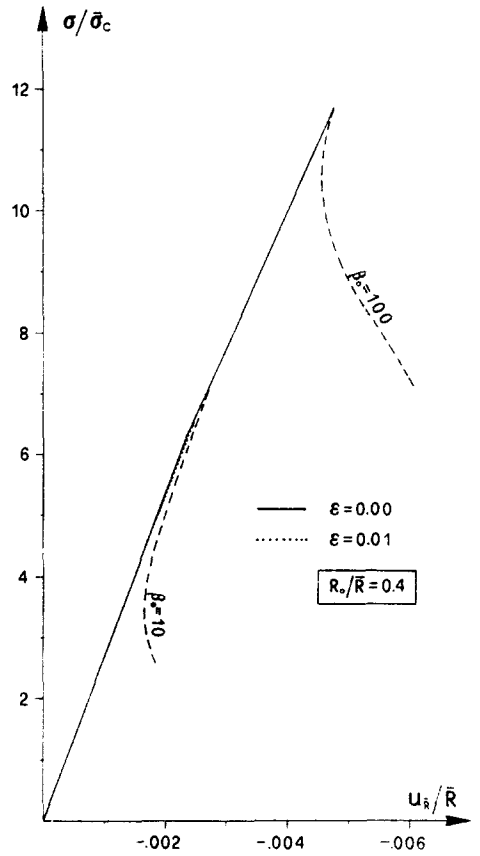

Fig. 11. Circular plate: analytical solution. External pressure edge σ versus axial displacement $u_{\bar{R}}$.

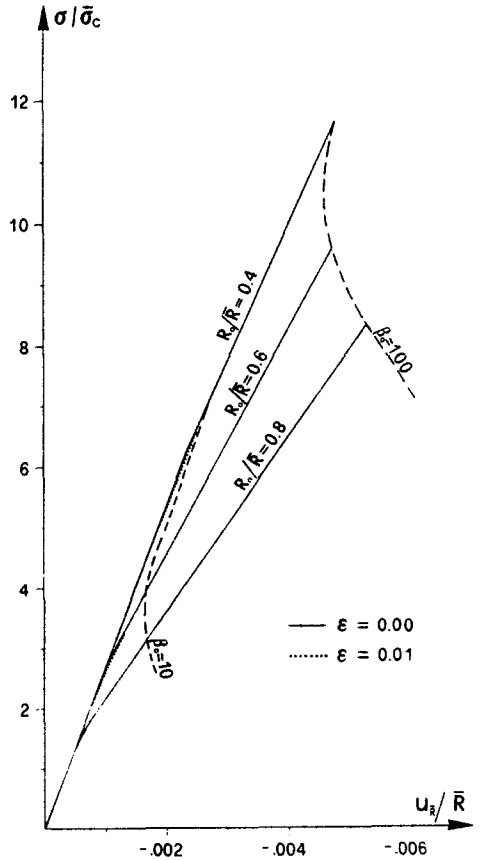

Fig. 12. Circular plate: analytical solution. External pressure edge σ versus axial displacement $u_{\bar{R}}$.

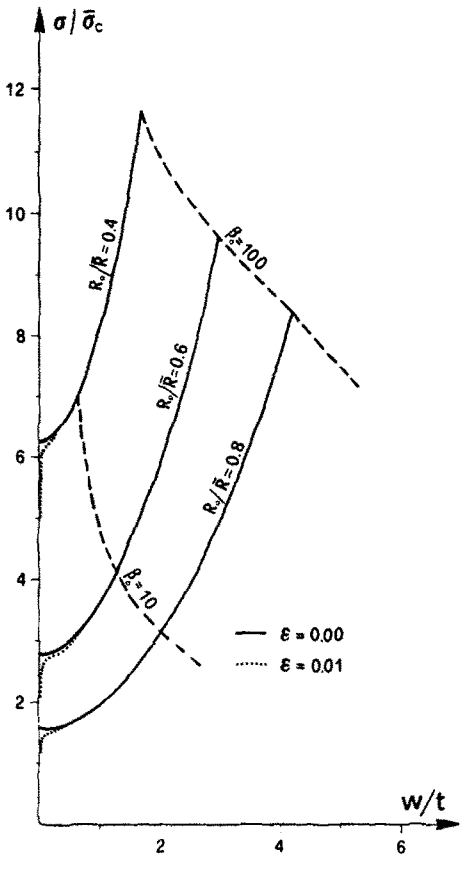

Fig. 13. Circular plate: analytical solution. External pressure edge σ versus central transverse deflection w.

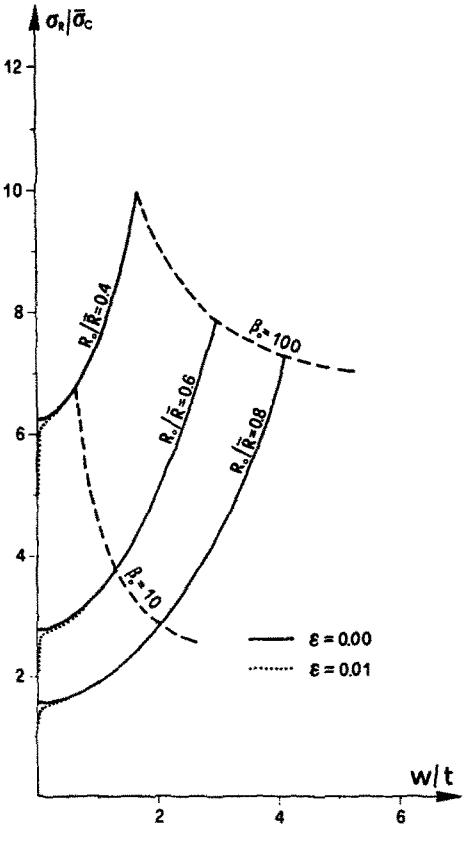

Fig. 14. Circular plate: analytical solution. Stress σ_R at the delamination front versus central transverse deflection w.

Figures 12 and 13 show similar results for different values of the initial debonding parameter $R_0/\bar{R} = 0.4, 0.6, 0.8$. In Figs 14 and 15, the relation between the stress σ_R at the delamination front is plotted versus the axial displacement u_R and the transverse deflection w.

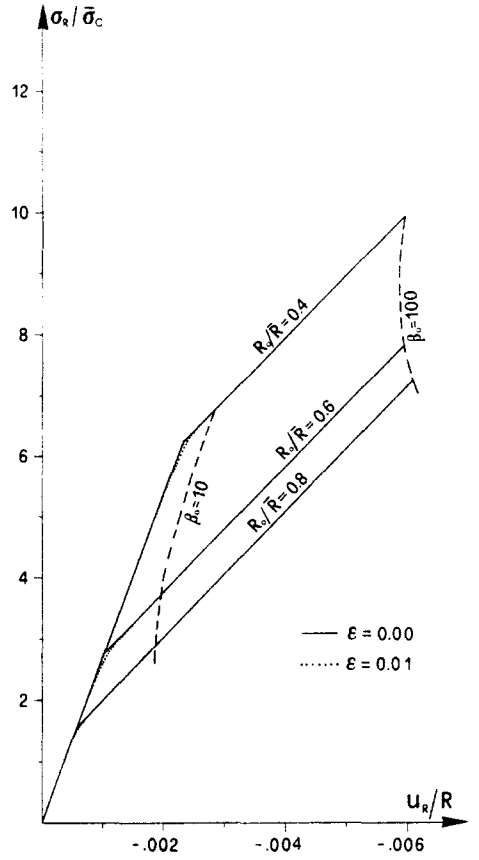

Fig. 15. Circular plate: analytical solution. Stress σ_R versus axial displacement u_R at the delamination front.

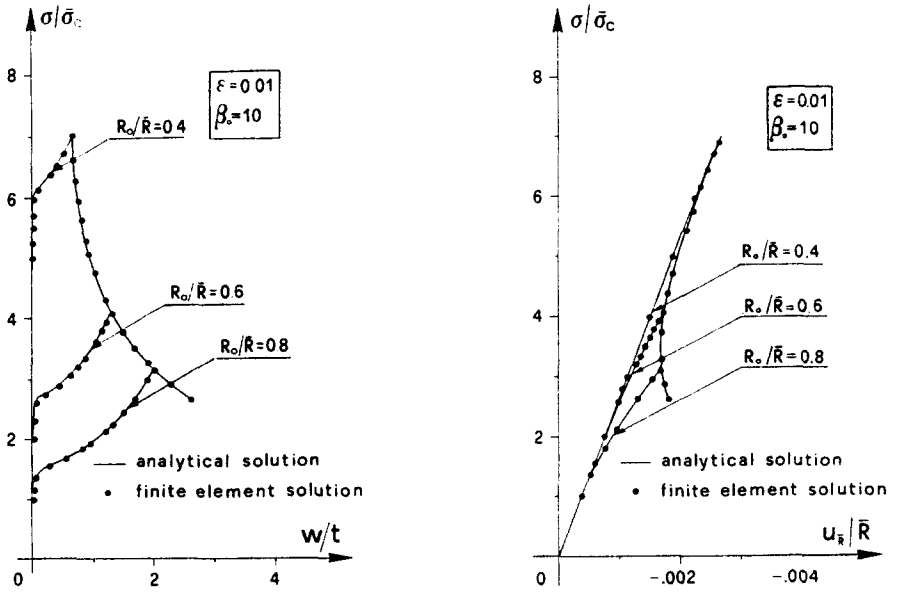

Fig. 16. Circular plate: comparison between analytical and numerical results.

In the previous figures the case of an initial small imperfection, corresponding to the parameter ε defined previously, is also examined.

The results show the small influence of the imperfection on the delamination process. On the basis of further numerical results we observed that for the circular plate, the influence of the imperfection can be neglected for values of ε less than 0.1.

In the work of Bottega and Maewal (1983) a similar example is considered, but the numerical results obtained are different from those shown in the previous figures. We observe that the delamination condition derived by Bottega and Maewal [eqn (28a)] is approximate because the first term appearing in our corresponding equation (34) is neglected. We also observe that the same approximation is contained in the example developed by Gillespie and Byron Pipes (1984), corresponding to our narrow plate example of Section 5. However, in this case the influence of the neglected terms is negligible.

In the case of the numerical analysis, a finite element technique, similar to that previously utilized for the narrow-plate example, is also used for the circular-plate example.

The finite element discretization is based on assumptions (i), (ii) and (iii) of Section 5.1 and the governing equilibrium equations, of the form (42), were derived from the stationary condition of the plate's potential energy functional:

$$\Phi = \sum_{N_e} \left\{ \pi D \int_{r_e}^{r_{e+1}} \left[w''^2 + \frac{2\nu}{r} w' w'' + \left(\frac{w'}{r}\right)^2 \right] r \, dr + \frac{\pi E t}{1-\nu^2} \int_{r_e}^{r_{e+1}} \left[(u' + \tfrac{1}{2}w'^2)^2 \right.\right.$$
$$\left.\left. + 2\nu(u' + \tfrac{1}{2}w'^2)\frac{u}{r} + \left(\frac{u}{r}\right)^2 \right] r \, dr + \pi \int_{r_e}^{r_{e+1}} k(w) w^2 r \, dr - 2\pi \int_{r_e}^{r_{e+1}} (q_u u + q_w w) r \, dr \right\}$$

where q_u and q_w represent axisymmetric axial and transverse loadings.

In Fig. 16 a comparison between the analytical results and the numerical ones is shown, for given values of the parameters involved in eqns (20), (30) and (35). These numerical results were obtained by the same finite element approach described for the first example problem discussed in Section 5.1, by assuming for the stiffness parameter $\bar{\tau} = k\bar{R}^4/D$ the value $\bar{\tau} = 10^{14}$. In this case also a good agreement between analytical and numerical solutions can be observed.

6. CONCLUSIONS

The postbuckling behaviour of two-layer plates with initial defects in bonding has been analyzed as a model problem in order to study delamination buckling in composite plates.

The force–displacement relation defining the delamination process has been examined by using an analytical solution, corresponding to the brittle fracture mechanics approach, and a finite element method which models debonding by means of unilateral springs.

A good matching is obtained between the analytical and numerical solutions. For the examined examples, the obtained results show that the delamination process is unstable, that is, occurring with decreasing external load.

It can also be observed that the finite element approach may be very useful in the analysis of two-dimensional problems in which the fracture mechanics approach is very difficult to apply.

REFERENCES

Ascione, L. and Bruno, D. (1983). On the delamination problem of two-layer plates. *Proc. II Meeting on Unilateral Problems in Structural Analysis*, Ravello, September 1983. CISM Courses and Lectures No. 288, 1–15. Springer, New York.

Bottega, W. G. and Maewal, A. (1983). Delamination buckling and growth in laminates. *J. Appl. Mech.* **50**, 184–189.

Budiansky, B. (1974). Theory of buckling and post-buckling behaviour of elastic structures. In *Advances in Applied Mechanics* (edited by Chia Shum Yih), Vol. 14, 1–65. Academic Press, New York.

Chai, H., Babcok, C. D. and Knauss, W. (1981). One dimensional modelling of failure in laminated plates by delamination buckling. *Int. J. Solids Structures* **17**, 1069–1083.

Early, J. W. (1981). Compression-induced delamination in a unidirectional graphite epoxy composite. Report MM-372A-81-14, Texas A & M University, College Station, Texas, U.S.A.

Evans, A. G. and Hutchinson, J. W. (1984). On the mechanics of delamination and spalling in compressed films. *Int. J. Solids Structures* **20**, 455–466.

Gillespie, J. W. Jr. and Byron Pipes, R. (1984). Compressive strength of composite laminates with interlaminar defects. *Composite Struct.* **2**, 41–69.

Grimaldi, A. and Reddy, J. N. (1982). On delamination in plates: a unilateral contact approach. Report VPJ-E-82-83, Virginia Polytechnic Institute and State University, Blacksburg, VA 24061, U.S.A.

Sterness, J. H. and Williams, J. R. (1983). Failure characteristic of graphite/epoxy components loaded in compression. *Proc. IUTAM Symp. on Mechanics of Composite Materials*, pp. 286–306. V.P.I., Blacksburg, U.S.A., 16–19 August 1982. Pergamon Press, Oxford/New York.

Thompson, J. M. T. and Hunt, G. W. (1973) *A General Theory of Elastic Stability*. Wiley-interscience, New York.

Yin, W. L., Sallam, N. and Simitses, J. (1986). Ultimate axial load capacity of a delaminate beam-plate. *AIAA J.* **24**(1), 123–128.